NUCLEAR INSTRUMENTS AND METHODS 57 (1967) 219–226; © NORTH-HOLLAND PUBLISHING CO.

THE CALIBRATION OF A Ge(Li) GAMMA-RAY SPECTROMETER FOR ENERGY AND RELATIVE INTENSITY MEASUREMENTS*

D. P. DONNELLY, H. W. BAER, J. J. REIDY and M. L. WIEDENBECK

University of Michigan, Ann Arbor, Michigan, U.S.A.

Received 17 July 1967

Two aspects of Ge(Li) gamma-ray spectrometry are discussed. The non-linearity of an amplifier-analyzer system was measured using a precision pulser and was checked with gamma-ray standards. The overall accuracy was 2 parts in 10^4. The relative detection efficiency of gamma-ray full-energy peaks was determined using sources with well measured relative gamma-ray emission rates. Two Ge(Li) detectors with active volumes of 3 $cm^2 \times 0.5$ cm and 4 $cm^2 \times 0.5$ cm were calibrated in the energy range 80–3200 keV. An overall accuracy of 5% in the energy region from 500–3200 keV and an accuracy of 10% over the entire range was obtained. The relative areas of the single escape peak and double escape peak to the full energy peak as a function of energy are included. The relative intensities of the 569.6, 1063.6 and 1771 keV gamma-rays following the decay of ^{207}Bi were measured.

1. Introduction

The usefulness of Ge(Li) gamma-ray spectrometers for nuclear decay scheme studies is well established. Consequently, the calibration of a Ge(Li) spectrometer for accurate measurements of gamma-ray energies and relative emission rates is of interest. A description of the determinations of non-linearities of the amplifier-analyzer system and relative detection efficiency is given here.

2. Experimental

2.1. Ge(Li) SPECTROMETER

The Ge(Li) spectrometers consisted of the following components: either an RCA detector, with depleted volume 3 $cm^2 \times 0.5$ cm, mounted in a cryostat constructed at the U. of M. machine shop or an Ortec detector-cryostat with depleted volume 4 $cm^2 \times 0.5$ cm; a Tennelec TC-130 (FET) pre-amp and TC-200 amplifier; and a Victoreen (Scipp) 1600 channel pulse-height analyzer. The best resolution at low count rates was obtained with the 1st differentiator and integrator time constants set at 1.6 μsec and 2nd differentiator time constant at 1 msec. The TC-130 and TC-200 units were modified to include pole-zero cancellation.

2.2. PULSER

The mercury pulser was constructed using a Power Designs model 2005 power supply and a 1 kΩ Fluke model 50 A/C potentiometer. A block diagram of the pulser is shown in fig. 1. The power supply has a measured voltage stability of about one part in 10^4 for periods of 1 h and one to four parts in 10^5 for periods of 10 min. The Fluke potentiometer calibration using a Biddle-Gray precision bridge indicates that the relative resistance values of the Fluke potentiometer are ac-

* Work supported in part by U.S. Atomic Energy Commission.

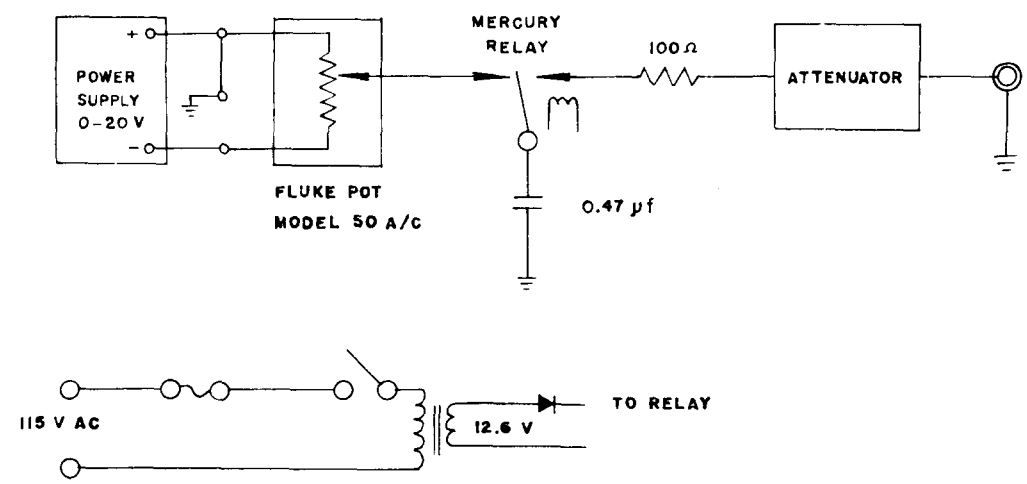

Fig. 1. A block diagram of the pulser.

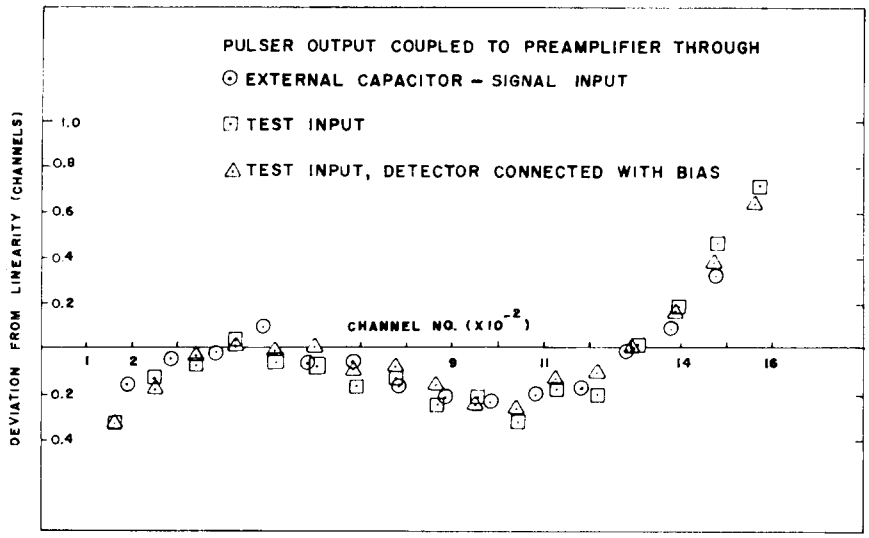

Fig. 2. A comparison of linearity calibrations with the pulser coupled to the preamplifier under three different conditions.

curate to within a few thousandths of an ohm. The mercury relay is operated at 60 cps so that each pulse occurs at a fixed phase in the power supply ripple, which is of the order of 100 μV. The capacitor has a polystyrene dielectric which shows good voltage recovery properties and a capacitance (0.47 μF) such that many time constants elapse in both the charging and discharging phases. The maximum impedance seen by the 0.47 μF capacitor in either the charging or discharging phase is 250 ohms; consequently the maximum RC combination allows at least 50 time constants to elapse before switching.

2.3. Source-detector arrangement

The source holders are lucite disks with a small depression for the source at the center. The source material was in all cases dissolved or suspended in a liquid, and was deposited with an eyedropper into the depression. The liquid was allowed to evaporate and the source was covered with scotch tape. The source disk was placed in a lucite source tower rigidly attached to the detector cryostat. Concentric source and detector alignment was achieved by use of cross hairs on the source tower, source-disk holder, and the front face of the cryostat. The source could be placed as close as 1 cm from the detector.

3. Determination of the amplifier-analyzer non-linearity

The pulser described above is coupled appropriately to the amplifier-analyzer system and 10^3–10^4 pulses are accumulated at 15–25 different pulse heights. The centroids of the pulser peaks are determined and the deviations from a straight line (determined by any one of various means) indicate the corrections to be applied to a data set. A check was made to see that the calibration was the same when the pulser was coupled to the input stage of the preamplifier through: 1. an external 1 pF capacitor; 2. the test input and 3. the test input with the detector connected and bias applied. The results shown in fig. 2 indicate that within the accuracy of the calibrations, the three are equivalent.

It was observed that the relative settings of the sensitivity control and the low level discriminator of the Victoreen Scipp 1600 multichannel analyzer could affect the linearity characteristics of the first few hundred channels above the analyzer cutoff. If the low level discriminator was set so that it rejected a range of pulses which passed the sensitivity limit, then the curve showing the deviation from linearity had a nearly parabolic shape as seen in fig. 4. If, however, the low level discriminator was set so that all pulses passing the sensitivity limit were analyzed, then the shape of the deviation curve is like the one seen in fig. 2. The shape of the deviation curve and the approximate channel number where the curvature changes depend on the specific settings of the low level discriminator and sensitivity control. The linearity characteristics were also found to depend on pulse polarity, and as expected, on the particular preamplifier and amplifier used.

A computer program was written so that a comparison of various data sets could be made. The program computed the centroid of each pulser peak, did a local interpolation of the data near channels 400 and 1300 to find the equivalent pulse heights at these points and then compared the input data with a line drawn through these points. This was done for purposes of

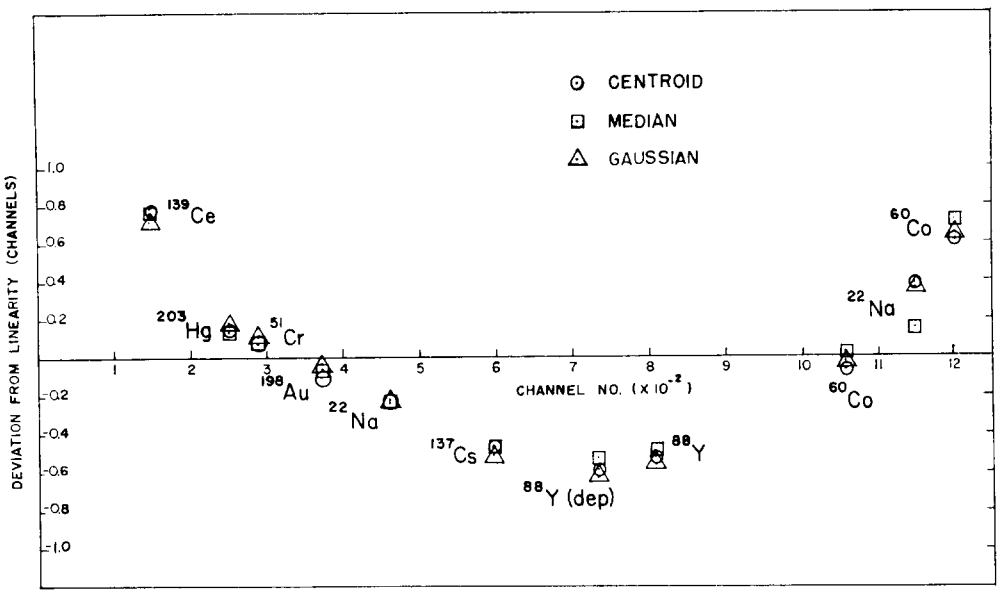

Fig. 3. A comparison of the deviations from linearity of a set of gamma-ray standards where the photopeaks are located using the centroid, median and a gaussian fit to the symmetric part of the peak.

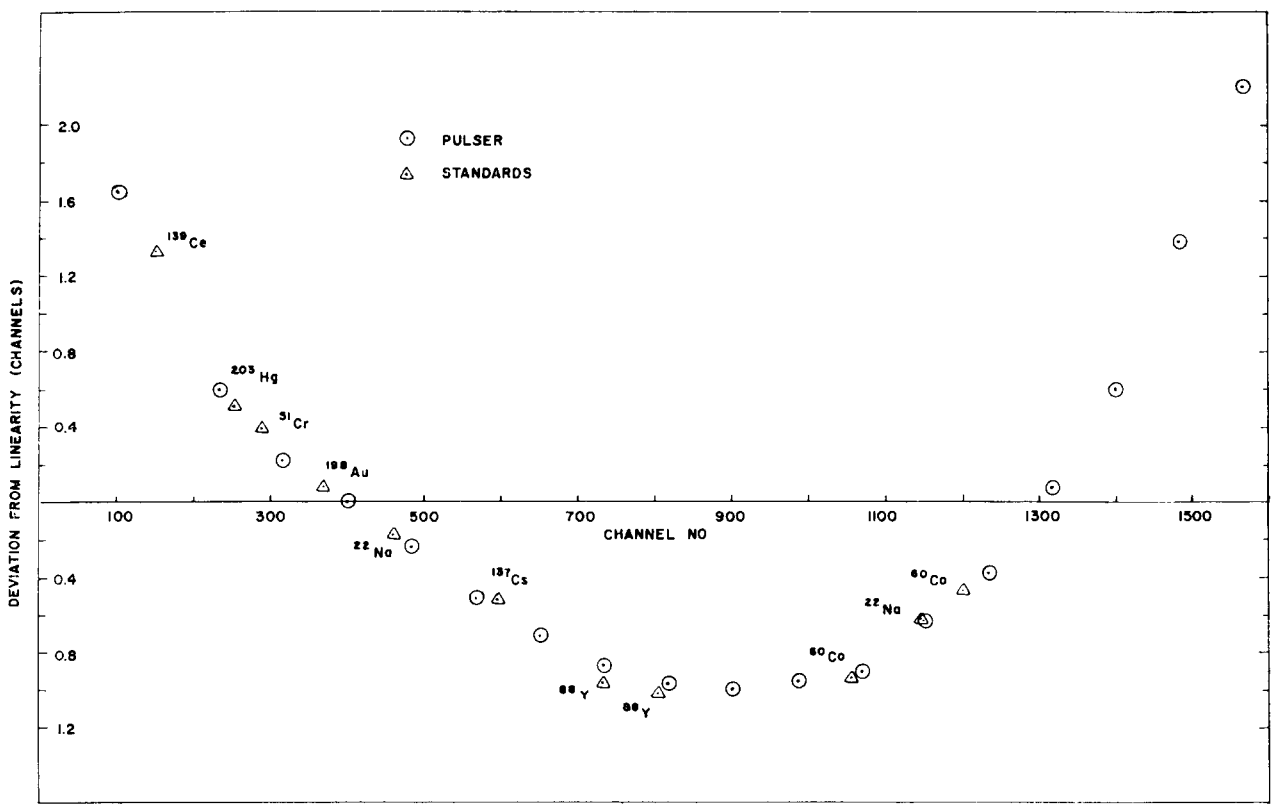

Fig. 4. A comparison of the deviations from linearity determined with the pulser and a set of gamma-ray standards.

TABLE 1
A comparison of calculated energies with measured energies.

Isotope (1)	Gamma-ray energy (keV) (2)	Corrected photopeak centroid (channels) (3)	Correction* (channels) (4)	Calc. energies from a least-squares fit to cols. 2 and 3 (keV) (5)	Diff. between cols. 2 and 5 (keV) (6)
^{139}Ce	165.856±0.008 [1] 165.85±0.05 [2]	150.211	1.25	165.802	0.054
^{203}Hg	279.18±0.02 [3]	252.178	0.51	279.168	0.012
^{51}Cr	320.085±0.006 [4] 320.07±0.05 [2]	288.958	0.35	320.059	0.026
^{198}Au	411.795±0.009 [5]	371.483	0.09	411.810	−0.015
^{22}Na	511.006±0.002 [6]	460.703	−0.18	511.004	0.002
^{137}Cs	661.632±0.076 [7]	596.201	−0.57	661.650	−0.018
^{88}Y	898.01±0.07 [2] 897.9±0.10 [8]	808.846	−0.96	898.07	−0.06
^{60}Co	1173.226±0.040 [9] 1173.25±0.08 [10]	1056.365	−0.90	1173.256	−0.030
^{22}Na	1274.52±0.07 [2] 1274.51±0.10 [8]	1147.411	−0.64	1274.48	0.04
^{60}Co	1332.483±0.046 [9] 1332.54±0.10 [10]	1199.548	−0.49	1332.446	0.037

* Calibration: 0.928 keV/channel.

comparison and is not necessary if one is simply interested in the corrections. Corrections can be obtained by determining deviations from a linear least-squares fit. However, if data points from various sets are not equal in number and/or spacing, comparison is not as convenient.

Before a check of the calibration method can be made, a parameter must be chosen to specify the position of a gamma-ray peak. The centroid, median and the mean of a gaussian fit to the symmetric part of the peak were determined. In fig. 3 the deviations of peak locations from a linear least squares fit are shown for the three cases. To within the present accuracy there does not appear to be a distinct advantage of one method over the others; consequently the centroid was chosen for convenience.

A comparison of the deviations from linearity for a typical run determined by using the pulser and a set of gamma-ray standards is shown in fig. 4. As a quantitative check, the deviations obtained from the pulser calibration were added to the centroids of the gamma-ray peak positions and a linear least-squares fit to the corrected peak locations and the known energies was performed. The results indicate that the corrections applied make the data linear overall to two parts in 10^4. An example of the applied corrections and resulting agreement is shown in table 1. It should be pointed out that, in one way or another, all currently used standard gamma-ray energy values are based on the rest-mass-energy of the electron and in some cases these standard energies have not been corrected to reflect the presently accepted value for the electron rest mass. However, the differences in the gamma-ray energies which would result from using the latest value of the electron rest mass are not significant in the present work.

As an alternate method for measuring non-linearities, a suitable set of gamma-ray standards can be used. The use of a set of gamma-ray standards permits using a counting rate approximating that of the source to be studied and eliminates the need for a pulser. However, the disadvantages of the standards method include a limited number of standards available in the region of interest, the time necessary to get good statistics in the gamma-ray spectrum and a more complicated analysis of the data.

4. Determination of the relative detection efficiency

4.1. Determination of the area of a peak

A graph showing the counting distribution in the ten or more channels adjacent to the base of the peak, was plotted for each peak. The shape of the distribution in these ten channels provided the basis for drawing a straight line which separated from the total spectral distribution that part of the distribution which was to be considered the peak. The area, A, of the peak is defined by the sum, $A = \sum_i (N_i - B_i)$ where N_i are the actual counts in a channel and B_i are the background counts in that channel as defined by the straight line.

The area obtained in this way depends on the manner in which the line is drawn and it is therefore important to follow a consistent procedure. By examining the trend of the distribution in the ten or more channels near the base of the peak, it was generally possible to ascertain to within one of two channels where the curvature of the distribution changed markedly. This marked change in curvature established the two points through which the straight line was drawn. The ratio of peak areas (taken for a set of 4–6 standards' spectra) derived in this way showed an rms fluctuation of about 1% for low counting rates. Since the uncertainties due to counting statistics could be made negligibly small, these fluctuations are considered to reflect variations in judgment in selecting the two points determining the straight lines. These fluctuations are of about the same magnitude as the uncertainties in the relative gamma-ray intensities used for the detection efficiency calibration. In view of this overall limit on the accuracy of the calibration, this method of determining peak areas was considered satisfactory. In complex spectra where the full-energy peaks are in general not as easily separated from the total distribution, care must be exercised to avoid making subjective errors. A possible check against this error is obtained by comparing the full energy peak profile after the background subtraction with a standard profile. Further, the extent of such a systematic error can be determined by drawing the separating straight line between different, but plausible, points at the base of the peak. From this range of peak areas one may deduce a reasonable uncertainty in that area.

4.2. The relative detection efficiency curve

The number of counts A in a full-energy peak is related to the emission rate of a gamma-ray with energy E, intensity I, from a source at a distance p from the detector, by the expression

$$A(E,p) = \eta'(E,p)\cdot\alpha(E,p)\cdot\Omega(p)It,$$

where I is the isotropic, gamma-ray emission rate/strad, $\Omega(p)$ the solid angle subtended by the detector, t the counting time and $\alpha(E,p)$ the attenuation factor representing the effects of absorbing layers between the source and detector. The function $\eta'(E,p)$ represents the fraction of gamma-rays in the solid angle that are detected in the full energy peak.

It is written as a function of p since edge effects are

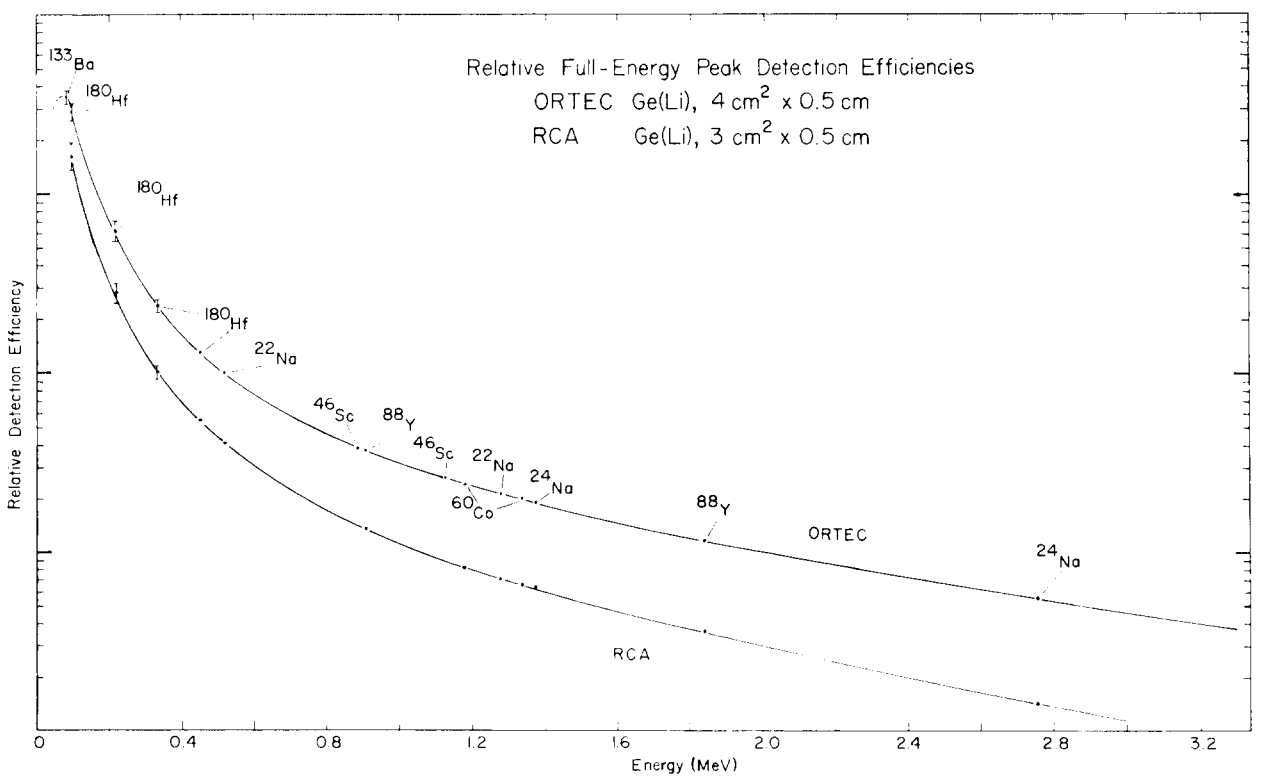

Fig. 5. The relative detection efficiency curves for two Ge(Li) detectors. The dimensions of the depleted volumes were provided by the manufacturers.

included in this term. In calibrating a particular source-detector arrangement it is desirable and convenient to combine the detection efficiency and attenuation terms into one function $\eta(E,p) = \eta'(E,p)\cdot\alpha(E,p)$. The ratio of two values of this function for gamma-ray energies E_1, E_2 can be written

$$R(E_1,E_2,p) = \eta(E_1,p)/\eta(E_2,p) = \\ = \{A(E_1,p)/A(E_2,p)\}(I_2/I_1).$$

The function $R(E_1,E_2,p)$ represents the relative full-energy peak detection efficiency for a particular source-detector arrangement. It was found that the relative areas for peaks in the standards' spectra were independent of p in the range 6 cm $\leqq p \leqq$ 20 cm, to within the accuracy the area ratio determination. The dependence for other values of p was not determined since the available source strengths were not convenient. Henceforth, the function $R(E_1,E_2,p)$ will be written $R(E_1,E_2)$ with the above range of p implied. The calibration of a source-detector arrangement is effected when the function $R(E_i,E_j)$ is determined for all values E_i,E_j within a certain range.

The calibration curves for the RCA and Ortec detectors are shown in fig. 5. The calibration range is approximately 80–3200 keV. The relative efficiency values of these two curves at the ^{22}Na ($E = 511$ keV) point are in the same ratio as the full energy peak areas in the spectra obtained with the two detectors at equal source to detector distances and equal counting times.

The two curves were obtained by using a pair-point method. The relative positions of pairs of points are adjusted graphically until a smooth curve can be drawn through them. Since there exist several standard sources with two gamma-rays having a relative emission rate known to about 1% or better, the pair-point method leads to an accuracy in the calibration which is somewhat better than is generally obtainable using sources with calibrated source strengths. In table 2 are listed the data pertinent to the efficiency calibration for the Ortec detector. In column one and two the relative gamma-ray rates are given. The related references for these values are given in column four. In column five are listed the relative full-energy-peak areas, $A(E_1)/A(E_2)$, for each pair of gamma-rays. The areas were determined as previously described. (For the case of ^{22}Na, a 1% correction was applied to account for absorption in the 0.13 cm thick Al surrounding the source, which assured that all the positions would annihilate at the source.) The uncertainties in the area ratios are rms deviations in the 3 to 6 runs taken with each source. Each source was run at various source to detector distances in the range 6–20 cm. In column six the relative detection efficiencies $\eta(E_1)/\eta(E_2)$ of each

TABLE 2
Data on the detection efficiency calibration for the Ortec detector.

Source (1)	E (MeV) (2)	Rel. emission rates* I_1/I_2 (3)	Ref. (4)	Full-energy peak area ratios+ $A(E_1)/A(E_2)$ (5)	Full-energy peak efficiency ratios $\eta(E_1)/\eta(E_2)$ (6)
^{22}Na	0.511 1.274	1.81(1 ± 0.01)	[11]	8.60(1 ± 0.01)	4.75(1 ± 0.014)
^{24}Na	1.368 2.753	1.00(1 ± 0.01)	[15]	3.39(1 ± 0.003)	3.39(1 ± 0.01)
^{60}Co	1.173 1.333	1.00(1 ± 0.01)	[11]	1.205(1 ± 0.01)	1.205(1 ± 0.014)
^{88}Y	0.898 1.836	0.940(1 ± 0.01)	[14]	3.04(1 ± 0·01)	3.23(1 ± 0.014)
^{46}Sc	0.889 1.120	1.00(1 ± 0.01)	[11]	1.46(1 ± 0.01)	1.46(1 ± 0.014)
^{180}Hf$^{(m)}$	0.093 0.215	0.200(1 ± 0.035)	[12]	0.925(1 ± 0.011)	4.63(1 ± 0.04)
	0.215 0.332	0.88(1 ± 0.05)	[12]	2.31(1 ± 0.013)	2.63(1 ± 0.05)
	0.332 0.448	1.15(1 ± 0.07)	[12]	2.10(1 ± 0.011)	1.83(1 ± 0.07)
^{133}Ba	0.081 0.356	0.52(1 ± 0.04)	[16]	9.07(1 ± 0.003)	17.4(1 ± 0.04)

* A 1% uncertainty in the relative emission rates has been adopted except for transitions in ^{180}Hf$^{(m)}$ and ^{133}Ba.
\+ The area ratio for ^{22}Na has been corrected for attenuation in the 0.13 cm thick Al surrounding the source.

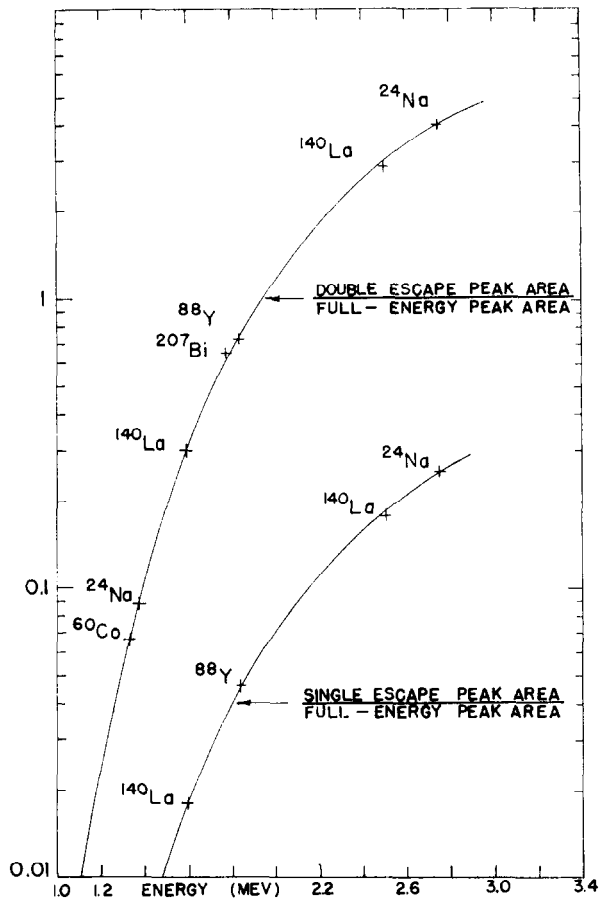

Fig. 6. Curves showing the single- and double-escape peak to full-energy peak area ratios for the Ortec detector.

pair of gamma-rays is listed. The uncertainty in the relative detection efficiency of each pair is due to two independent contributions: the uncertainty in the relative gamma-ray emission rate and the uncertainty in the relative areas.

In the region between 0.50 to 2.8 MeV in which there are ten data points, the maximum overall uncertainty is estimated to be about 5%. The uncertainty in the relative detection efficiency for smaller energy intervals is of course smaller, and for the case in which the relative detection efficiency of two gamma-rays with energies close to that of a pair of points used in the calibration is desired, the uncertainty is about 1% (in the interval 0.5 to 2.8 MeV). In the interval 80 to 500 keV the uncertainty in the curve is large, due to the uncertainty in the relative intensities of the ^{180}Hf gamma-rays (3–7%). Thus the overall uncertainty in this portion of the efficiency curve is about 10%, while for smaller intervals it is less.

It should be pointed out that the relative efficiency curve obtained in this way represents the overall relative efficiency of the source-detector system, and includes the effects of the various absorbing layers. One may compare this curve with the theoretical curves obtained by the Monte Carlo method. If the efficiency curve for the Ortec detector (0.5 cm depletion depth, 2.3 cm dia.) is compared with the theoretical intrinsic efficiency curves [18]) for the 0.5, 0.8 cm depletion depth detectors (1.8 cm dia.), it is observed that the curvatures in the region 400–1500 keV are very nearly the same. In the region below 400 keV the theoretical curves rise more sharply than the experimental curve. Absorbing layers account for a part of this deviation. At 200 keV, 6–7% of the γ-rays are absorbed.

When analyzing complex spectra it is sometimes useful to know the ratios of the single and double escape peak areas to the full energy peak areas. Two such curves are shown in fig. 6 for the Oretec detector. These data were not compared with the results[18]) since these curves are expected to be strongly dependent on detector geometry. One does not expect such a strong dependence for relative photopeak efficiency curves.

5. The relative intensity of γ-rays in the decay of ^{207}Bi

As a first application of the efficiency curve (Ortec), the relative intensities of three gamma-rays in the decay of ^{207}Bi were measured. This source (30 y half-life) has three lines conveniently spaced for efficiency calibrations. Three runs were taken and the intensities of the three strongest lines were determined as described above. The results of this measurement together with those of other investigations are shown in table 3. The intensity values given by Raeside and Ludington[19]) were determined using a 17 cm^3 coaxial Ge(Li) detector which was calibrated in this laboratory in a manner similar to that described above.

The authors wish to express their appreciation to I. P. Auer for computing the gaussian fit to the gamma-ray photopeaks, to E. Arnold and W. Wing for helpful comments on the pulser design and to S. Lee for assistance in the collection and analysis of data. We

TABLE 3
Data on gamma-rays in the ^{207}Bi→^{207}Pb decay.

E(keV)	Relative gamma-ray intensities			
	Present	ref.[13])	ref.[15])	ref.[19])
569.62±0.06 [17])	100	100	100	100
1063.63±0.07 [2])	78.4±2.4	78	77±3	78.3±2.4
1771	7.07±0.35	8	9±1	7.27±0.44

also thank D. Raeside and M. Ludington for communicating their experimental results and R. Mosher of the electrical engineering department for the calibration of the potentiometer.

References

[1]) H. W. Baer, private communication.
[2]) W. W. Black and R. L. Heath, Nucl. Physics A**90** (1964) 650.
[3]) C. J. Herrlander and R. L. Graham, Nucl. Physics **58** (1964) 544.
[4]) J. J. Reidy, private communication.
[5]) G. Murray, R. L. Graham and J. S. Geiger, Nucl. Physics **45** (1963) 177.
[6]) E. R. Cohen and J. W. M. DuMond, Rev. Mod. Phys. **37** (1965) 537.
[7]) R. L. Graham, G. T. Ewan and J. S. Geiger, Nucl. Instr. and Meth. **9** (1960) 245.
[8]) A. V. Ramayya, J. H. Hamilton, S. M. Brahmavar and J. J. Pinajian, Phys. Letters **24B** (1967) 49.
[9]) G. Murray, R. L. Graham and J. S. Geiger, Nucl. Physics **63** (1965) 353.
[10]) J. J. Reidy and M. L. Wiedenbeck, Bull. Am. Phys. Soc. **10** (1965) 1131.
[11]) J. M. Freeman and J. G. Jenkin, Nucl. Instr. and Meth. **43** (1966) 269.
[12]) W. F. Edwards and F. Boehm, Phys. Rev. **121** (1961) 1499.
[13]) D. E. Alburger and A. W. Sunyar, Phys. Rev. **99** (1955) 695.
[14]) R. W. Peelle, Oak Ridge National Laboratory, Report ORNL-3016 (1960).
[15]) R. Van Lieshout, A. H. Wapstra, R. A. Ricci and R. K. Girgis in *Alpha-, Beta- and Gamma-ray spectroscopy* (ed. K. Siegbahn; North-Holland Publ. Co., Amsterdam, 1965) p. 504.
[16]) K. C. Mann and R. P. Chaturvedi, Can. J. Phys. **41** (1963) 932.
[17]) F. P. Brady, N. F. Peak and R. A. Warner, Nucl. Physics **66** (1965) 365.
[18]) N. V. DeCastro Faria and R. J. A. Levesque, Nucl. Instr. and Meth. **46** (1967) 325.
[19]) D. Raeside and M. Ludington, private communication.